

Orbital angular momentum in a topological superconductor with Chern number higher than 1

Atsuo Shitade¹ and Yuki Nagai²

¹*Yukawa Institute for Theoretical Physics, Kyoto University, Kyoto 606-8502, Japan**

²*CCSE, Japan Atomic Energy Agency, 178-4-4, Wakashiba, Kashiwa, Chiba, 277-0871, Japan*

(Dated: May 26, 2016)

We investigate the bulk orbital angular momentum (AM) in a two-dimensional hole-doped topological superconductor (SC) which is composed of a hole-doped semiconductor thin film, a magnetic insulator, and an s -wave SC and is characterized by the Chern number $C = -3$. In the topological phase, L_z/N is strongly reduced from the intrinsic value by the non-particle-hole-symmetric edge states as in the corresponding chiral f -wave SCs when the spin-orbit interactions (SOIs) are small, while this reduction of L_z/N does not work for the large SOIs. Here L_z and N are the bulk orbital AM and the total number of particles at zero temperature, respectively. As a result, L_z/N is discontinuous or continuous at the topological phase transition depending on the strengths of the SOIs. We also discuss the effects of the edge states by calculating the radial distributions of the orbital AM.

PACS numbers: 74.20.-z, 74.20.Rp

I. INTRODUCTION

Orbital angular momentum (AM) is one of the most fundamental quantities in classical and quantum mechanics. In condensed matter physics, the bulk orbital AM in chiral superconductors (SCs) has been intensively studied^{1–20}. A chiral SC is an exotic SC whose Cooper pairs carry nonzero orbital AM ℓ , and hence the time-reversal symmetry is spontaneously broken. ³He-A is the only material experimentally established as a chiral superfluid, whose pairing symmetry is chiral p wave¹⁵. Also, Sr₂RuO₄ is widely believed to be a chiral p -wave SC^{21,22}. Therefore, most of the previous studies have focused on chiral p wave and at least theoretically concluded $L_z/N = +1/2$ in an ideal situation, where L_z and N are the bulk orbital AM and the total number of particles at zero temperature, respectively^{1–13}. In general, chiral SCs with ℓ are expected to have $L_z/N = \ell/2$ without an edge or a vortex¹³, which we call the intrinsic value.

Recently, it was found that the bulk orbital AM in two-dimensional chiral SCs with $\ell > 1$ is remarkably reduced as $L_z/N = o(1)$ ^{18–20}. In two dimensions, chiral SCs are gapped and are topological SCs characterized by the Chern number $C = \ell$ and the presence of the Majorana edge states. When $\ell = 1$, only one edge state is particle-hole symmetric (PHS) by itself and is called the PHS edge state¹⁸. On the other hand, when $\ell > 1$ is even, each edge state is PHS with another but not PHS by itself. Such edge states are called the non-PHS edge states¹⁸. When $\ell > 1$ is odd, there are the PHS and non-PHS edge states. The non-PHS edge states give rise to the nonzero spectral asymmetry and reduce the bulk orbital AM from the intrinsic value $L_z/N = \ell/2$. Although chiral d or f wave has been proposed in UPt₃²³, URu₂Si₂^{24–27}, and SrPtAs^{28–30}, the theory cannot be applied to these three-dimensional materials with nodes directly.

Apparently, the above reduction of the bulk orbital AM requires not $\ell > 1$ but $C > 1$. Realization of two-dimensional time-reversal broken topological SCs with $C > 1$ is classified into two types. The first type is intrinsic, namely, without impurities, and can be realized in a quantum anomalous Hall insulator in proximity to an s -wave SC³¹, a heterostructure of

a hole-doped semiconductor thin film, a magnetic insulator, and an s -wave SC³², and the systems with the help of p -wave SCs^{33–35}. The second type relies on impurities and can be realized in a lattice of magnetic impurities on the surface of an s -wave SC with the Rashba spin-orbit interaction (SOI)^{36,37} and that of nonmagnetic impurities in a chiral p -wave SC³⁸. In these proposals, arbitrarily high Chern numbers are available in principle. In return for using a conventional s -wave SC, SOIs play an important role in generating the effective chirality of Cooper pairs. Among these proposals, a hole-doped topological SC proposed in Ref. 32 is a natural extension of an electron-doped topological SC composed of an electron-doped semiconductor thin film, a magnetic insulator, and an s -wave SC^{39–41} and offers an experimentally feasible system to verify the theory of the bulk orbital AM. We note that hole-doped semiconductors accompanied by ferromagnetism can be realized by Mn doping and are called dilute magnetic semiconductors^{42,43}. However, it is not trivial how the bulk orbital AM is reduced in this system because the orbital AM is not conserved in the presence of the SOIs.

In this paper, we investigate the bulk orbital AM in a hole-doped topological SC³² comparing with that in an electron-doped topological SC^{39–41}. We calculate the bulk orbital AM both by the Green's function formula¹³ and on a circular disk. As mentioned above, the non-PHS edge states dramatically reduce the bulk orbital AM in the case of $C > 1$. In addition, Tsutsumi and Machida pointed out that $L_z/N = +1/2$ in chiral p -wave SCs consists of $L_z^{\text{MJ}}/N = +1$ from the Majorana edge state and $L_z^{\text{cont}} = -1/2$ from the continuum states¹². The authors already found that L_z/N in an electron-doped topological SC is continuous at the topological phase transition and is nonzero even in the trivial phase which does not support the Majorana edge state⁴⁴. Therefore it is important to reveal the difference of the contributions to the bulk orbital AM from the PHS edge, non-PHS edge, and continuum states. We also discuss the effects of the SOIs which are indispensable for topological SCs.

We find that the conserved quantity is modified by SOIs. When the Chern number is higher than 1, it can be nonzero owing to the presence of the non-PHS edge states and the

nonzero spectral asymmetry, which results in the reduction of the bulk orbital AM as shown in Refs. 18–20. Since the bulk orbital AM calculated in the reciprocal space is continuous at the topological phase transition, that calculated in the real space shows a jump. Differently from the existing literature, this reduction is not universal and can be tuned by SOIs in this system.

II. MODEL

First, we review a hole-doped topological SC composed of a hole-doped semiconductor thin film, a magnetic insulator, and an s -wave SC³²,

$$\begin{aligned} \mathcal{H}_{\vec{k}} = & [\xi_{1k} - \sqrt{3}\xi_{2k}(\Gamma_4 \cos 2\phi + \Gamma_3 \sin 2\phi) \\ & + (\xi_{2k} - W)\Gamma_5 + 2\alpha k(j_y \cos \phi - j_x \sin \phi)]\tau_z - 2h j_z \\ & + [(\Delta_H - \Delta_L)/2 + (\Delta_H + \Delta_L)\Gamma_5/2]\tau_x, \end{aligned} \quad (1)$$

where we choose the Nambu basis, $\Psi_{\vec{k}} = [c_{\vec{k}+3/2}, c_{\vec{k}+1/2}, c_{\vec{k}-1/2}, c_{\vec{k}-3/2}, c_{-\vec{k}-3/2}^\dagger, c_{-\vec{k}-1/2}^\dagger, c_{-\vec{k}+1/2}^\dagger, c_{-\vec{k}+3/2}^\dagger]^\top$. $\vec{\tau}$ is a set of the Pauli matrices for the Nambu space, and \vec{j} is the total AM of $j = 3/2$ holes but is called spin to avoid confusion below. We use the standard representation,

$$j_x = \begin{bmatrix} & \sqrt{3}/2 & & \\ \sqrt{3}/2 & & 1 & \\ & 1 & & \sqrt{3}/2 \\ & & \sqrt{3}/2 & \end{bmatrix}, \quad (2a)$$

$$j_y = \begin{bmatrix} & -\sqrt{3}i/2 & & \\ \sqrt{3}i/2 & & -i & \\ & i & & -\sqrt{3}i/2 \\ & & \sqrt{3}i/2 & \end{bmatrix}, \quad (2b)$$

$$j_z = \begin{bmatrix} 3/2 & & & \\ & 1/2 & & \\ & & -1/2 & \\ & & & -3/2 \end{bmatrix}, \quad (2c)$$

and construct the Γ matrices satisfying the anticommutation relations $\{\Gamma_a, \Gamma_b\} = 2\delta_{ab}$ ⁴⁵,

$$\Gamma_1 = \{j_y, j_z\} / \sqrt{3} = \begin{bmatrix} & -i & & \\ i & & & \\ & & i & \\ & & & -i \end{bmatrix}, \quad (3a)$$

$$\Gamma_2 = \{j_z, j_x\} / \sqrt{3} = \begin{bmatrix} & 1 & & \\ 1 & & & \\ & & -1 & \\ & & & 1 \end{bmatrix}, \quad (3b)$$

$$\Gamma_3 = \{j_x, j_y\} / \sqrt{3} = \begin{bmatrix} & -i & & \\ & & -i & \\ i & & & \\ & i & & \end{bmatrix}, \quad (3c)$$

$$\Gamma_4 = (j_x^2 - j_y^2) / \sqrt{3} = \begin{bmatrix} & 1 & & \\ & & 1 & \\ 1 & & & \\ & 1 & & \end{bmatrix}, \quad (3d)$$

$$\Gamma_5 = j_z^2 - 5/4 = \begin{bmatrix} 1 & & & \\ & -1 & & \\ & & -1 & \\ & & & 1 \end{bmatrix}. \quad (3e)$$

The first, second, and third terms in Eq. (1) are the two-dimensional Luttinger Hamiltonian, which describes a hole-doped semiconductor thin film⁴⁶. We define $\xi_{1k} = \gamma_1 k^2 / 2m - \mu$ and $\xi_{2k} = \gamma_2 k^2 / 2m$, in which $\vec{k} = k[\cos \phi, \sin \phi]$ is a two-dimensional wavevector, γ_1 and γ_2 are the Luttinger parameters, and μ is the chemical potential. In a hole-doped semiconductor, confinement into a quantum well yields quantization of momentum $\langle k_z \rangle = 0$ and $\langle k_z^2 \rangle \neq 0$ and opens up the gap $W = \gamma_2 \langle k_z^2 \rangle / m$ between the heavy-hole bands with $j_z = \pm 3/2$ and the light-hole bands with $j_z = \pm 1/2$. This point is a crucial difference from an electron-doped semiconductor, in which confinement just shifts the chemical potential. The fourth and fifth terms are the Rashba SOI and the Zeeman interaction, respectively, and the sixth and seventh terms are the s -wave pairing potentials induced by the proximity effect. Note that we neglect some terms allowed by the theory of invariants⁴⁶.

The topological phase transitions occur when the gap closes at $k = 0$. We can analytically obtain eight eigenvalues, $\pm 3h \pm \sqrt{(\mu + W)^2 + \Delta_H^2}$ and $\pm h \pm \sqrt{(\mu - W)^2 + \Delta_L^2}$, and two phase transition lines, $3h_{\text{cH}} = \sqrt{(\mu + W)^2 + \Delta_H^2}$ and $h_{\text{cL}} = \sqrt{(\mu - W)^2 + \Delta_L^2}$, where the Chern number changes by -3 and -1 , respectively. The phase diagrams for different Δ_H and Δ_L are shown in Fig. 1. $C = -3$ is realized when the chemical potential lies in the lowest heavy-hole band alone, which is described by the cubic Rashba model with the Zeeman interaction in the large- W limit³². We should note that the gap may accidentally close at $k \neq 0$, which does not change the Chern number.

Below we put $\gamma_1 = 1$, $\gamma_2 = 0.3$, $m = 0.5$, $\mu = 0$, $W = 1$, $\Delta_H = -\Delta_L = 1$ focusing on Fig. 1(a), leading to $h_{\text{cH}} = 0.47$ and $h_{\text{cL}} = 1.41$. Once we choose energy and wavenumber units, the remaining important parameters are γ_2/γ_1 , μ/W , $2m\alpha^2/\gamma_1 W$, h/W , Δ_H/W , and Δ_L/W . Among these, Δ_H/W and Δ_L/W drastically change the phase diagram as shown in Fig. 1. Here we arbitrarily choose $\Delta_H/W = -\Delta_L/W = 1$ since we cannot estimate their experimental values. γ_2/γ_1 takes 0.2-0.4 for typical III-V semiconductors such as GaAs⁴⁷, and hence our choice of $\gamma_2/\gamma_1 = 0.3$ is realistic. μ/W can be tuned experimentally by doping carriers or applying an external field. Note that W is about 16meV for a GaAs quantum well with 100Å thickness.

III. METHODS

We calculate the bulk orbital AM in two ways. One is based on the Green's function formula in the reciprocal space¹³. Since there is no edge state in the periodic boundary condition, we do not discuss the effects of the non-PHS edge states but interpret the resulting bulk orbital AM as the intrinsic value.

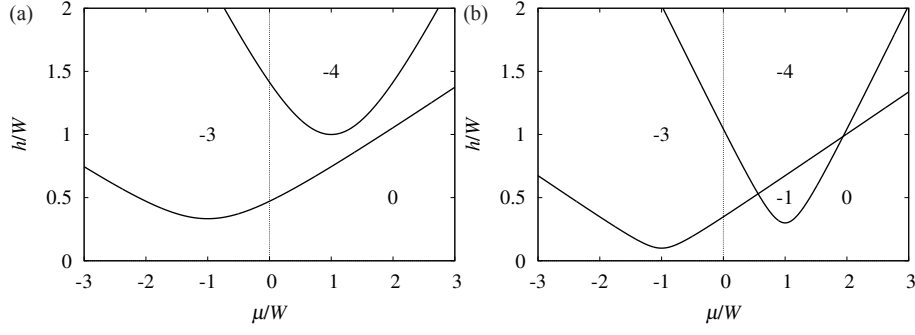


FIG. 1. Phase diagrams in terms of the Chern number for (a) $|\Delta_H/W| = |\Delta_L/W| = 1$ and (b) $|\Delta_H/W| = |\Delta_L/W| = 0.35$.

Here we calculate the Hall viscosity $2\eta_H$, which is known to be equal to the bulk orbital AM L_z in two-dimensional gapped systems at zero temperature^{48–50}. By using the Matsubara Green's function $\mathcal{G}(i\omega_n, \vec{k}) = (i\omega_n - \mathcal{H}_{\vec{k}})^{-1}$, the Chern number⁵¹ and the Hall viscosity¹³ can be evaluated by

$$C = \frac{1}{6i} \epsilon_{abc} \int \frac{d^3k}{(2\pi)^2} \text{tr} \mathcal{G} \partial_{k_a} \mathcal{G}^{-1} \mathcal{G} \partial_{k_b} \mathcal{G}^{-1} \mathcal{G} \partial_{k_c} \mathcal{G}^{-1}, \quad (4a)$$

$$2\eta_H = \frac{1}{12i} \epsilon_{abc} \int \frac{d^3k}{(2\pi)^3} \vec{k}^2 \text{tr} \mathcal{G} \partial_{k_a} \mathcal{G}^{-1} \mathcal{G} \partial_{k_b} \mathcal{G}^{-1} \mathcal{G} \partial_{k_c} \mathcal{G}^{-1}. \quad (4b)$$

Here we introduce $k_0 = i\omega_n$, and ϵ_{abc} is the totally antisymmetric tensor with $\epsilon_{012} = 1$. Although the integrals are carried out over the $(i\omega_n, \vec{k})$ space, the prefactor \vec{k}^2 in Eq. (4b) is in two dimensions.

The other way is a straightforward calculation in the real space. We solve the Bogoliubov-de Gennes (BdG) equation $\mathcal{H}_{-\vec{r}} \Psi_{\ell i}(\vec{r}) = E_{\ell i} \Psi_{\ell i}(\vec{r})$ on a disk with its radius R . Since the system preserves the rotational symmetry, the BdG wave function can be expressed as

$$\Psi_{\ell i}(\vec{r}) = (2\pi)^{-1/2} e^{i\ell\phi} [u_{\ell i 0}(r), e^{i\phi} u_{\ell i 1}(r), e^{2i\phi} u_{\ell i 2}(r), e^{3i\phi} u_{\ell i 3}(r), v_{\ell i 0}(r), e^{i\phi} v_{\ell i 1}(r), e^{2i\phi} v_{\ell i 2}(r), e^{3i\phi} v_{\ell i 3}(r)]^T, \quad (5)$$

and the radial BdG equation is written by

$$[-(\gamma_1 + \gamma_2)\mathcal{L}_{\ell}(r)/2m - \mu - W - 3h]u_{\ell i 0}(r) - \sqrt{3}\alpha\mathcal{R}_{\ell+1}(r)u_{\ell i 1}(r) + (\sqrt{3}\gamma_2/2m)\mathcal{S}_{\ell+2}(r)u_{\ell i 2}(r) + \Delta_H v_{\ell i 0}(r) = E_{\ell i} u_{\ell i 0}(r), \quad (6a)$$

$$\sqrt{3}\alpha\mathcal{R}_{-\ell}(r)u_{\ell i 0}(r) + [-(\gamma_1 - \gamma_2)\mathcal{L}_{\ell+1}(r)/2m - \mu + W - h]u_{\ell i 1}(r) - 2\alpha\mathcal{R}_{\ell+2}(r)u_{\ell i 2}(r) + (\sqrt{3}\gamma_2/2m)\mathcal{S}_{\ell+3}(r)u_{\ell i 3}(r) - \Delta_L v_{\ell i 1}(r) = E_{\ell i} u_{\ell i 1}(r), \quad (6b)$$

$$(\sqrt{3}\gamma_2/2m)\mathcal{S}_{-\ell}(r)u_{\ell i 0}(r) + 2\alpha\mathcal{R}_{-(\ell+1)}(r)u_{\ell i 1}(r) + [-(\gamma_1 - \gamma_2)\mathcal{L}_{\ell+2}(r)/2m - \mu + W + h]u_{\ell i 2}(r) - \sqrt{3}\alpha\mathcal{R}_{\ell+3}(r)u_{\ell i 3}(r) - \Delta_L v_{\ell i 2}(r) = E_{\ell i} u_{\ell i 2}(r), \quad (6c)$$

$$(\sqrt{3}\gamma_2/2m)\mathcal{S}_{-(\ell+1)}(r)u_{\ell i 1}(r) + \sqrt{3}\alpha\mathcal{R}_{-(\ell+2)}(r)u_{\ell i 2}(r) + [-(\gamma_1 + \gamma_2)\mathcal{L}_{\ell+3}(r)/2m - \mu - W + 3h]u_{\ell i 3}(r) + \Delta_H v_{\ell i 3}(r) = E_{\ell i} u_{\ell i 3}(r), \quad (6d)$$

$$[-(\gamma_1 + \gamma_2)\mathcal{L}_{\ell}(r)/2m - \mu - W + 3h]v_{\ell i 0}(r) + \sqrt{3}\alpha\mathcal{R}_{\ell+1}(r)v_{\ell i 1}(r) - (\sqrt{3}\gamma_2/2m)\mathcal{S}_{\ell+2}(r)v_{\ell i 2}(r) + \Delta_H u_{\ell i 0}(r) = E_{\ell i} v_{\ell i 0}(r), \quad (6e)$$

$$-\sqrt{3}\alpha\mathcal{R}_{-\ell}(r)v_{\ell i 0}(r) - [-(\gamma_1 - \gamma_2)\mathcal{L}_{\ell+1}(r)/2m - \mu + W + h]v_{\ell i 1}(r) + 2\alpha\mathcal{R}_{\ell+2}(r)v_{\ell i 2}(r) - (\sqrt{3}\gamma_2/2m)\mathcal{S}_{\ell+3}(r)v_{\ell i 3}(r) - \Delta_L u_{\ell i 1}(r) = E_{\ell i} v_{\ell i 1}(r), \quad (6f)$$

$$-(\sqrt{3}\gamma_2/2m)\mathcal{S}_{-\ell}(r)v_{\ell i 0}(r) - 2\alpha\mathcal{R}_{-(\ell+1)}(r)v_{\ell i 1}(r) - [-(\gamma_1 - \gamma_2)\mathcal{L}_{\ell+2}(r)/2m - \mu + W - h]v_{\ell i 2}(r) + \sqrt{3}\alpha\mathcal{R}_{\ell+3}(r)v_{\ell i 3}(r) - \Delta_L u_{\ell i 2}(r) = E_{\ell i} v_{\ell i 2}(r), \quad (6g)$$

$$-(\sqrt{3}\gamma_2/2m)\mathcal{S}_{-(\ell+1)}(r)v_{\ell i 1}(r) - \sqrt{3}\alpha\mathcal{R}_{-(\ell+2)}(r)v_{\ell i 2}(r) - [-(\gamma_1 + \gamma_2)\mathcal{L}_{\ell+3}(r)/2m - \mu - W - 3h]v_{\ell i 3}(r) + \Delta_H u_{\ell i 3}(r) = E_{\ell i} v_{\ell i 3}(r), \quad (6h)$$

Here we introduce $\mathcal{L}_{\ell}(r) \equiv \partial_r^2 + (1/r)\partial_r - \ell^2/r^2$, $\mathcal{R}_{\ell+1}(r) \equiv \partial_r + (\ell+1)/r$, and $\mathcal{S}_{\ell+2}(r) \equiv \partial_r^2 + [(2\ell+3)/r]\partial_r + \ell(\ell+2)/r^2$. We impose the boundary conditions $g'(0) = g(R) = 0$ ($g = u_{\ell i m}, v_{\ell i m}$) and the normalization condition,

$$\int_0^R r dr [\mathbf{u}_{\ell i}^2(r) + \mathbf{v}_{\ell i}^2(r)] = 1. \quad (7)$$

Owing to the PHS $\mathcal{H}_{\vec{k}} = -C\mathcal{H}_{-\vec{k}}^*C^\dagger$ with $C = -ie^{i\pi j_y}\tau_y$, when the BdG wave function Eq. (5) has the eigenvalue $E_{\ell i}$,

$$C\Psi_{\ell i}^*(\vec{r}) = (2\pi)^{-1/2}e^{-i(\ell+3)\phi}[-v_{\ell i3}, e^{i\phi}v_{\ell i2}, -e^{2i\phi}v_{\ell i1}, e^{3i\phi}v_{\ell i0}, u_{\ell i3}, -e^{i\phi}u_{\ell i2}, e^{2i\phi}u_{\ell i1}, -e^{3i\phi}u_{\ell i0}]^T, \quad (8)$$

has the eigenvalue $-E_{\ell i}$. Therefore we only have to solve the radial BdG equation Eq. (6) for $\ell \geq -1$. The total number of particles N , the total spin J_z , and the bulk orbital AM L_z can be calculated by

$$N = \sum_{\ell=-1}^{\ell_{\max}} \sum_i \int_0^R r dr [\mathbf{u}_{\ell i}^2(r)f(E_{\ell i}) + \mathbf{v}_{\ell i}^2(r)f(-E_{\ell i})], \quad (9a)$$

$$J_z = \sum_{\ell=-1}^{\ell_{\max}} \sum_i \int_0^R r dr [\mathbf{u}_{\ell i}^T(r)j_z\mathbf{u}_{\ell i}(r)f(E_{\ell i}) - \mathbf{v}_{\ell i}^T(r)j_z\mathbf{v}_{\ell i}(r)f(-E_{\ell i})], \quad (9b)$$

$$L_z = \sum_{\ell=-1}^{\ell_{\max}} (\ell + 3/2) \sum_i \int_0^R r dr [\mathbf{u}_{\ell i}^2(r)f(E_{\ell i}) - \mathbf{v}_{\ell i}^2(r)f(-E_{\ell i})] - J_z, \quad (9c)$$

respectively, in which $f(z) = \theta(-z)$ is the Fermi-Dirac distribution function at $T = 0$. We use the central difference method with N_g grid points, which reduces a set of the differential equations Eq. (6) to the $8N_g \times 8N_g$ eigenvalue problem. We put the disk radius $R = 50$, the number of grid points $N_g = 500$, and the AM cutoff $\ell_{\max} = 512 - 2$. Figure 2 shows the low-energy spectra for $C = 0, -3, -4$. There are one PHS edge mode and one pair of the non-PHS edge modes in Fig. 2(b), which results from $C = -3$. On the other hand, there are two pairs of the non-PHS edge modes in Fig. 2(c), which results from $C = -4$.

IV. RESULTS

Figure 3 shows the h and α dependences of the total spin J_z/N and the bulk orbital AM L_z/N obtained by the real and reciprocal spaces. We find that J_z/N obtained by the real space always coincides with that by the reciprocal space, while L_z/N obtained by the real space is reduced compared with that by the reciprocal space for $h > h_{\text{CH}}$. Therefore these two are denoted by $L_z^{(r)}/N$ and $L_z^{(k)}/N$, respectively, below. This reduction of the bulk orbital AM is expected from the previous studies^{18–20} but not strong when h is small or α is large. This mechanism and quantitative criterion are discussed later. We also find $L_z^{(k)}/N + J_z/N = 0$ as in an electron-doped topological SC⁴⁴.

Owing to the presence of the SOIs, not the orbital AM ℓ_z but the total AM $i_z = \ell_z + j_z$ is conserved. In the reciprocal space, we can easily check

$$[\ell_z, \mathcal{H}_{\vec{k}}] = -[j_z, \mathcal{H}_{\vec{k}}] = 2i[\sqrt{3}\xi_{2k}(\Gamma_3 \cos 2\phi - \Gamma_4 \sin 2\phi) + \alpha k(j_x \cos \phi + j_y \sin \phi)]\tau_z, \quad (10)$$

and $[i_z, \mathcal{H}_{\vec{k}}] = 0$ for each \vec{k} . Therefore the eigenstates are the simultaneous eigenstates of i_z . By summing up the eigenvalues of i_z over the negative-energy eigenstates, we obtain the bulk total AM $I_z^{(k)} = L_z^{(k)} + J_z = 0$. Such discussion holds only when the negative-energy eigenstates are well defined,

namely, the system is gapped. In the real space, Eq. (9) is rewritten as

$$\begin{aligned} L_z^{(r)} + J_z &= -\frac{1}{2} \sum_{\ell=-1}^{\ell_{\max}} (\ell + 3/2) \sum_i [f(-E_{\ell i}) - f(E_{\ell i})] \\ &\quad + \frac{1}{2} \sum_{\ell=-1}^{\ell_{\max}} (\ell + 3/2) \sum_i \int_0^R r dr [\mathbf{u}_{\ell i}^2(r) - \mathbf{v}_{\ell i}^2(r)] \\ &= -\frac{1}{2} \sum_{\ell=-1}^{\ell_{\max}} (\ell + 3/2) \eta_\ell, \end{aligned} \quad (11)$$

by using the spectral asymmetry,

$$\eta_\ell \equiv \sum_i [f(-E_{\ell i}) - f(E_{\ell i})]. \quad (12)$$

This is similar to the previous results on chiral SCs^{5,18,19} but is modified by the presence of the SOIs⁵². For $C = -3$ as shown in Fig. 2(b), the non-PHS edge states cross $E = 0$ at $\pm(\ell_F + 3/2)/R$ with ℓ_F being called the Fermi AM¹⁸, which leads to the nonzero spectral asymmetry $\eta_\ell = -2$ for $0 < (\ell + 3/2)/R < (\ell_F + 3/2)/R$ and reduces the bulk orbital AM by $\Delta L_z^{(r)} = (\ell_F + 2)^2/2$.

Differently from chiral SCs, the reduction of the bulk orbital AM depends on h and α through the Fermi AM. To see this, we show the h and α dependences of the Fermi AM normalized by $N^{1/2}$ in Fig. 4 since we are interested not in $\Delta L_z^{(r)}$ but in $\Delta L_z^{(r)}/N$. We find that the Fermi AM is large enough to reduce the bulk orbital AM almost to zero for $(\lambda_L^2 + h^2)/2\lambda_L < W - \mu$ but is small in the opposite case, leading to $L_z^{(k)}/N \simeq L_z^{(r)}/N$. Here $\lambda_L \equiv m(2\alpha/\sqrt{3})^2/(\gamma_1 + 2\gamma_2)$ is the effective strength of the Rashba SOI for the light-hole bands. The factor $2/\sqrt{3}$ comes from the matrix elements in j_x and j_y . This is because the sharp decrease of the Fermi AM around $\alpha = 1$ is accompanied by the Lifshitz transition in the normal state. The lowest particle band is always one of the heavy-hole bands with $j_z = +3/2$, but the second lowest particle band changes from the other heavy-hole band with $j_z = -3/2$ to

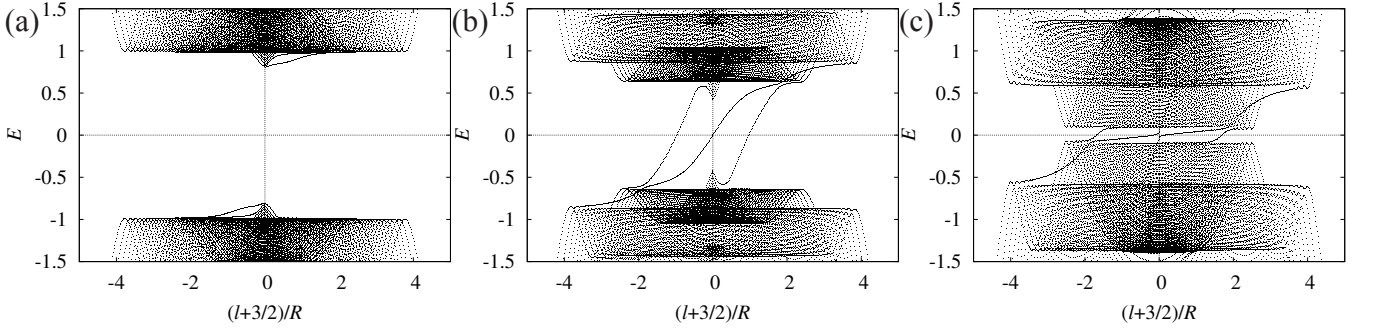


FIG. 2. Spectra for (a) $h = 0.2 < h_{cH}$ ($C = 0$), (b) $h_{cH} < h = 1 < h_{cL}$ ($C = -3$), and (c) $h = 2 > h_{cL}$ ($C = -4$). We put $\alpha = 1.5$.

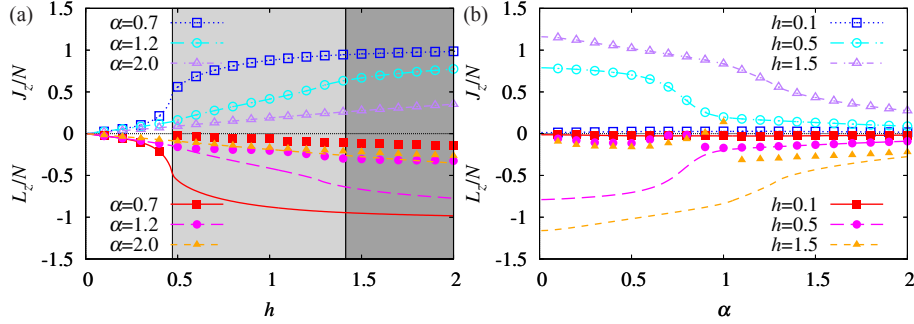


FIG. 3. (Color online) (a) h and (b) α dependences of the total spin J_z/N and the bulk orbital AM $L_z^{(r)}/N$. Symbols and lines are obtained by the real and reciprocal spaces, respectively. In (a), the light and dark gray regions indicate the topological phases with $C = -3, -4$, respectively.

one of the light-hole bands with $j_z = +1/2$ at $h = W/2$. In order to realize the topological phase with $C = -3$, $k = 0$ of the second lowest particle band should be above from the chemical potential. However, when the strength of the Rashba SOI overcomes the Zeeman interaction, this light-hole band has its minimum at $k \neq 0$, and hence the Lifshitz transition can occur as shown in Fig. 5. The non-PHS edge states connect the heavy-hole band with the antiparticle counterpart of the light-hole band before the Lifshitz transition. Once the Lifshitz transition occurs, the non-PHS edge states connect the heavy-hole band with the inner part of the antiparticle counterpart of the light-hole band, which leads to the sharp decrease of the Fermi AM.

The h and α dependences of the bulk orbital AM in the reciprocal space $L_z^{(k)}/N$ in a hole-doped topological SC can be understood in the same way as those in an electron-doped topological SC⁴⁴. We translate the previous results for electrons to heavy holes. To do this, we define the effective strength of the Rashba SOI for heavy holes by $\lambda_H \equiv ma^2/(\gamma_1 - 2\gamma_2)$. For the small SOIs $2\lambda_H(\mu + W) + (3h)^2 < \Delta_H^2$ in the trivial phase, the s -wave pairing potential is dominant, and hence we obtain $L_z^{(k)}/N \simeq 0$. For $\lambda_H < 3h$ in the topological phase with $C = -3$, we expect $L_z^{(k)}/N \simeq -3/2$ from the $(f - if)$ -wave pairing potential. In between, $L_z^{(k)}/N$ rapidly increases even in the trivial phase since the s -wave pairing potential is no longer dominant due to the Pauli depairing effect, and the $(f \mp if)$ -wave pairing potentials coexist. For the large SOIs $\lambda_H > 3h$, spins are tilted in the xy plane, and $L_z^{(k)}/N$ is sup-

pressed through the conservation law $L_z^{(k)} + J_z = 0$. Note that $L_z^{(k)}/N$ shown in Fig. 3(b) does not reach $-3/2$ even for $\lambda_H < 3h$ because the Zeeman interaction does not overcome the other SOI $\gamma_2 = 0.3$.

To summarize these results, the h dependence of the bulk orbital AM is intriguing for the small SOIs as shown in Fig. 3(a). First, the system is trivial due to the s -wave pairing potential, and $L_z^{(r)}/N = L_z^{(k)}/N$ is almost zero. Second, the system is still trivial due to the coexistence of the $(f \mp if)$ -wave pairing potentials, and $L_z^{(r)}/N = L_z^{(k)}/N$ rapidly increases. Finally, the system turns into the topological phases with $C = -3, -4$, and only $L_z^{(r)}/N$ is strongly reduced by the non-PHS edge states. Thus the h dependence of $L_z^{(r)}/N$ in a hole-doped topological SC is nonmonotonic in contrast to that in an electron-doped topological SC. On the other hand, for $2\lambda_H(\mu + W) + (3h)^2 > \Delta_H^2$, the system starts from the coexisting region. In the topological phases, the reduction of $L_z^{(r)}/N$ does not work due to the Lifshitz transition in the second lowest particle band and the sharp decrease of the Fermi AM. Therefore the h dependence of $L_z^{(r)}/N \simeq L_z^{(k)}/N$ is almost monotonic and gradual since $L_z^{(k)}/N = -J_z/N$ is suppressed by the large SOIs $\lambda_H > 3h$.

V. DISCUSSION

So far, we have concentrated on the bulk orbital AM altogether. Here we discuss how the PHS edge, non-PHS edge,

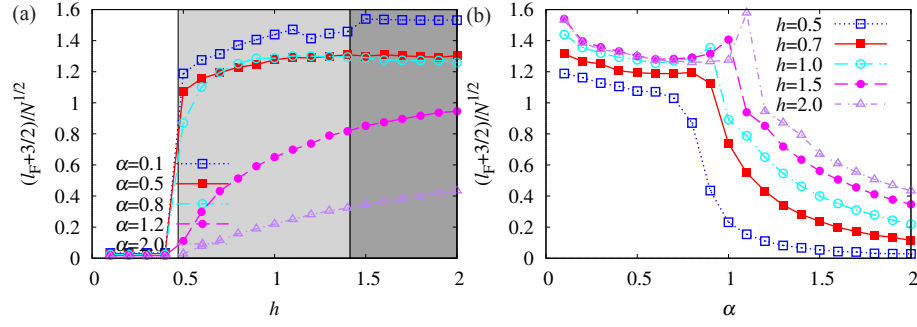


FIG. 4. (Color online) (a) h and (b) α dependences of the Fermi AM. For $C = -4$, only the outer Fermi AM is shown because the inner Fermi AM is found to be small. In (a), the light and dark gray regions indicate the topological phases with $C = -3, -4$, respectively.

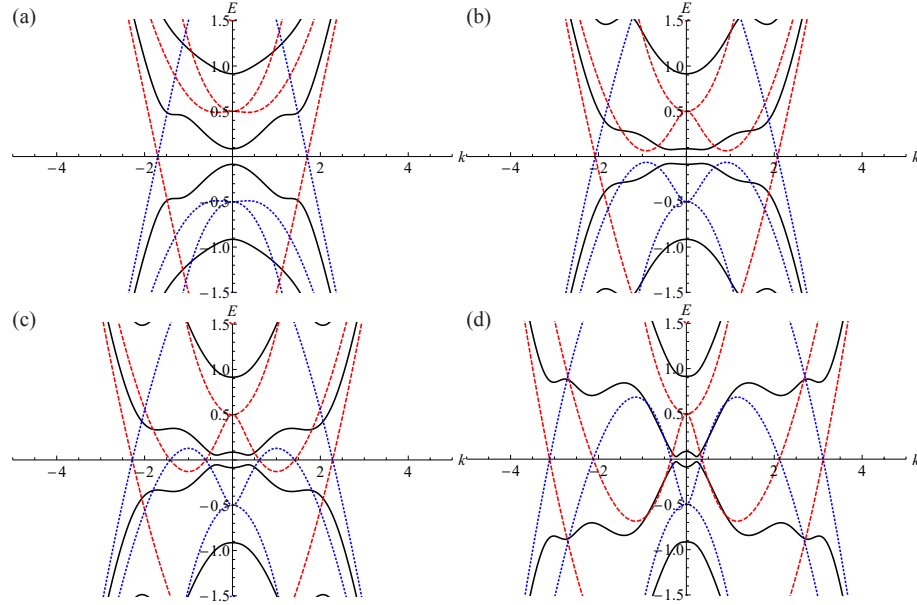


FIG. 5. (Color online) Black solid line indicates the band structure for the BdG Hamiltonian Eq. (1), while red broken and blue dotted lines indicate the electron and hole bands in the normal state, respectively. We set $h = 0.5$ and (a) $\alpha = 0.5$, (b) $\alpha = 0.8$, (c) $\alpha = 0.9$, (d) $\alpha = 1.2$. Between (b) and (c), the Fermi AM shows the sharp decrease in Fig. 4(b).

and continuum states contribute to the bulk orbital AM separately. The first and second lowest positive-energy eigenstates are continuum states in the trivial phase and become one of the non-PHS edge states and the PHS edge state, respectively, in the topological phase with $C = -3$. We can reveal the effects of the PHS and non-PHS edge states more clearly by decomposing the bulk orbital AM with respect to the index of eigenstates around the topological phase transition. Equation (9c) is decomposed as

$$\begin{aligned} L_z^{(r)} &= \int_0^R r dr \ell_z^{(r)}(r) \\ &= \int_0^R r dr [\ell_z^{i=2}(r) + \ell_z^{i=1}(r) + \ell_z^{i \neq 1,2}(r)]. \end{aligned} \quad (13)$$

Remember that we have $8N_g$ eigenstates labeled by $i = -4N_g + 1, \dots, 0, 1, 2, \dots, 4N_g$, $\ell_z^{i=2}(r)$, $\ell_z^{i=1}(r)$, $\ell_z^{i \neq 1,2}(r)$ are dubbed the PHS edge, non-PHS edge, and continuum con-

tributions, respectively, in the case of $C = -3$, as shown in Fig. 2(b). In the case of $C = 0$ as shown in Fig. 2(a), all of them originate from the continuum states.

In the context of chiral p -wave SCs, Tsutsumi and Machida previously showed that the bulk orbital AM $L_z/N = -1/2$ consists of $L_z^{\text{MJ}}/N = -1$ from the PHS edge state and $L_z^{\text{cont}}/N = 1/2$ from the continuum states and pointed out that these contributions can be experimentally distinguished by controlling the edge roughness¹². Thus the PHS edge state is expected to play an important role for the bulk orbital AM. As shown in Ref. 44 and Fig. 3(a), the bulk orbital AM increases in the trivial phase and does not jump at the topological phase transition apart from the reduction by the non-PHS edge states, which indicates that the continuum contribution may change its sign from negative to positive at the topological phase transition.

First, we carry out a similar analysis for an electron-doped topological SC, which is designed to be a chiral p -wave SC with use of the Rashba SOI³⁹⁻⁴¹, in order to compare with a

chiral p -wave SC and a hole-doped topological SC of our interest. We set $\alpha = 0.1$ to focus on its chiral p -wave behavior and change h around the phase transition point $h_c = 0.61$. See Ref. 44 for the Hamiltonian and the other parameters we set. In Fig. 6, we show the radial distributions $\ell_z^{i=1}(r)$ and $\ell_z^{i\neq 1}(r)$. For $C = -1$, the PHS edge contribution $\ell_z^{i=1}(r)$ in Fig. 6(b) and the continuum contribution $\ell_z^{i\neq 1}(r)$ in Fig. 6(c) are negative and positive, respectively, which is consistent with the previous result obtained by the quasiclassical Eilenberger theory¹². However, we cannot find any significant difference between before and after the topological phase transition. The $i = 1$ eigenstate, which goes down toward $E = 0$ and turns into the PHS edge state for $h > h_c$, is already localized at the edge even for $h < h_c$ and has the negative orbital AM. Therefore, as L_z^{MJ}/N from the PHS edge state in a chiral p -wave SC is expected to be fragile against the edge roughness¹², not only the orbital AM from the PHS edge state in the topological phase but also that from one of the continuum states in the trivial phase is expected to be fragile.

Now let us move on to a hole-doped topological SC. Figure 7 shows the radial distributions $\ell_z^{i=2}(r)$, $\ell_z^{i=1}(r)$, $\ell_z^{i\neq 1,2}(r)$. We set $\alpha = 0.7$ to avoid the accidental gap closing at $k \neq 0$ and to focus on its chiral f -wave behavior. In Fig. 7(b), the orbital AM of the $i = 2$ eigenstate, which turns into the PHS edge state for $h > h_{\text{CH}}$, shows no significant difference between before and after the topological phase transition as in an electron-doped topological SC. On the other hand, the radial distribution from the $i = 1$ eigenstate, which goes across $E = 0$ and turns into the non-PHS edge state for $h > h_{\text{CH}}$, discontinuously decreases at the topological phase transition. This decrease is associated with the discontinuous reduction of the bulk orbital AM $\Delta L_z > 0$. Note that the radial distribution is not positive because this eigenstate has the negative orbital AM even in the trivial phase similar to the $i = 2$ eigenstate. Thus the effect of the non-PHS edge states can be found not in the radial distribution itself but in its change at the topological phase transition.

VI. SUMMARY

In conclusion, we have investigated the bulk orbital AM in a two-dimensional topological SC which is composed of a hole-doped semiconductor, a ferromagnet, and an s -wave SC and is characterized by $C = -3$. We have obtained $L_z^{(k)}/N$ by using the Green's function formula of the Hall viscosity in the reciprocal space and $L_z^{(r)}/N$ by solving the BdG equation on a circular disk.

Our findings are as follows: (1) Before the topological phase transition, $L_z^{(r)}/N = L_z^{(k)}/N$ starts to increase as in an electron-doped topological SC⁴⁴. (2) For $\lambda_L < W - \mu$, $L_z^{(r)}/N$ is reduced from $L_z^{(k)}/N$ almost to zero owing to the non-PHS edge states with the large Fermi AM, which is expected from the recent studies on chiral SCs with $\ell > 1$ ^{18–20}. As a consequence, $L_z^{(r)}/N$ is nonmonotonic as a function of the Zeeman interaction. (3) In the opposite case, the Fermi AM of the non-PHS edge states becomes small associated with the Lifshitz transition in the normal state, and the reduction of the bulk orbital AM does not work. (4) This effect competes with the other effect to tilt spins and suppress the bulk orbital AM. Thus a hole-doped topological SC offers an experimentally feasible stage to investigate the bulk orbital AM in chiral f -wave SCs and the interesting deviations due to the SOIs.

Finally, let us comment on other models of two-dimensional topological SCs previously proposed. SOIs are the most important ingredients throughout this paper, which make the system topological and modify the conserved quantity. The models without use of SOIs^{34,35,38} are out of our scope. The explicit form of the conserved quantity depends on the details of the system as studied in Ref. 52, but it is given by $L_z + S_z$ at least for the models in Refs. 31 and 33. Therefore we expect that our findings (1), (2), and (4) above are generic for these models with $C > 1$. On the other hand, our finding (3) is quite specific to a hole-doped topological SC which makes use of $j = 3/2$ holes. We also note that the Fermi AM and the reduction of the bulk orbital AM can be controlled by a confinement potential⁵².

ACKNOWLEDGMENTS

A. S. was supported by the Japan Society for the Promotion of Science (JSPS) KAKENHI Grant No. 25287085, and Y. N. was partially supported by JSPS KAKENHI Grant No. 26800197.

* Present address: RIKEN Center for Emergent Matter Science, 2-1 Hirosawa, Wako, Saitama 351-0198, Japan

¹ M. Ishikawa, Prog. Theor. Phys. **57**, 1836 (1977).

² M. G. McClure and S. Takagi, Phys. Rev. Lett. **43**, 596 (1979).

³ N. D. Mermin and P. Muzikar, Phys. Rev. B **21**, 980 (1980).

⁴ M. Ishikawa, K. Miyake, and T. Usui, Prog. Theor. Phys. **63**, 1083 (1980).

⁵ G. E. Volovik, JETP Lett. **61**, 958 (1995).

⁶ T. Kita, J. Phys. Soc. Jpn. **67**, 216 (1998).

⁷ J. Goryo and K. Ishikawa, Phys. Lett. A **246**, 549 (1998).

⁸ M. Stone and R. Roy, Phys. Rev. B **69**, 184511 (2004).

⁹ T. Mizushima, M. Ichioka, and K. Machida, Phys. Rev. Lett. **101**, 150409 (2008).

¹⁰ T. Mizushima and K. Machida, Phys. Rev. A **81**, 053605 (2010).

¹¹ J. A. Sauls, Phys. Rev. B **84**, 214509 (2011).

¹² Y. Tsutsumi and K. Machida, Phys. Rev. B **85**, 100506 (2012).

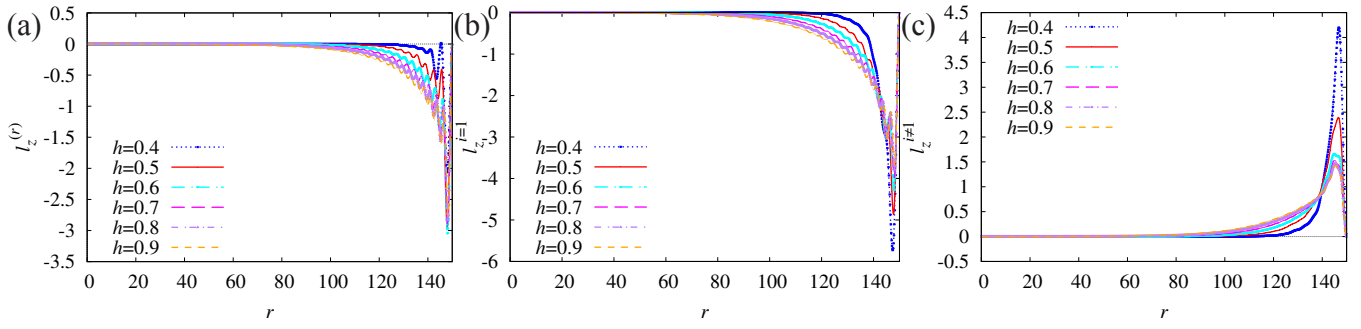


FIG. 6. (Color online) Radial distributions of (a) $\ell_z^{(r)}(r)$, (b) $\ell_z^{i=1}(r)$, and (c) $\ell_z^{i \neq 1}(r)$ for $h < h_c = 0.61$ ($C = 0$) and $h > h_c$ ($C = -1$) in an electron-doped topological SC. We set $\alpha = 0.1$. See Ref. 44 for the other parameters.

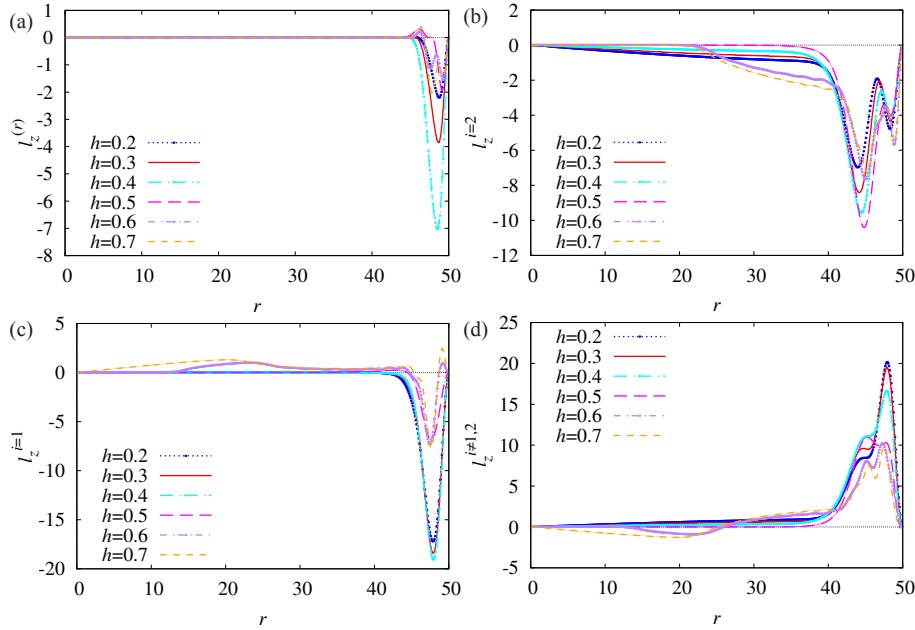


FIG. 7. (Color online) Radial distributions of (a) $\ell_z^{(r)}(r)$, (b) $\ell_z^{i=2}(r)$, (c) $\ell_z^{i=1}(r)$, and (d) $\ell_z^{i \neq 1,2}(r)$ for $h < h_{cH} = 0.47$ ($C = 0$) and $h > h_{cH}$ ($C = -3$) in a hole-doped topological SC. We set $\alpha = 0.7$.

- ¹³ A. Shitade and T. Kimura, Phys. Rev. B **90**, 134510 (2014).
- ¹⁴ P. W. Anderson and P. Morel, Phys. Rev. **123**, 1911 (1961).
- ¹⁵ A. J. Leggett, Rev. Mod. Phys. **47**, 331 (1975).
- ¹⁶ G. E. Volovik, JETP Lett. **22**, 108 (1975).
- ¹⁷ M. C. Cross, J. Low Temp. Phys. **21**, 525 (1975).
- ¹⁸ Y. Tada, W. Nie, and M. Oshikawa, Phys. Rev. Lett. **114**, 195301 (2015).
- ¹⁹ G. E. Volovik, JETP Lett. **100**, 742 (2014).
- ²⁰ W. Huang, E. Taylor, and C. Kallin, Phys. Rev. B **90**, 224519 (2014).
- ²¹ A. P. Mackenzie and Y. Maeno, Rev. Mod. Phys. **75**, 657 (2003).
- ²² Y. Maeno, S. Kittaka, T. Nomura, S. Yonezawa, and K. Ishida, J. Phys. Soc. Jpn. **81**, 011009 (2012).
- ²³ R. Joynt and L. Taillefer, Rev. Mod. Phys. **74**, 235 (2002).
- ²⁴ Y. Kasahara, T. Iwasawa, H. Shishido, T. Shibauchi, K. Behnia, Y. Haga, T. D. Matsuda, Y. Onuki, M. Sigrist, and Y. Matsuda, Phys. Rev. Lett. **99**, 116402 (2007).
- ²⁵ K. Yano, T. Sakakibara, T. Tayama, M. Yokoyama, H. Amit-suka, Y. Homma, P. Miranović, M. Ichioka, Y. Tsutsumi, and K. Machida, Phys. Rev. Lett. **100**, 017004 (2008).
- ²⁶ Y. Kasahara, H. Shishido, T. Shibauchi, Y. Haga, T. D. Matsuda, Y. Onuki, and Y. Matsuda, New J. Phys. **11**, 055061 (2009).
- ²⁷ H. Kusunose, J. Phys. Soc. Jpn. **81**, 023704 (2012).
- ²⁸ J. Goryo, M. H. Fischer, and M. Sigrist, Phys. Rev. B **86**, 100507 (2012).
- ²⁹ P. K. Biswas, H. Luetkens, T. Neupert, T. Stürzer, C. Baines, G. Pascua, A. P. Schnyder, M. H. Fischer, J. Goryo, M. R. Lees, H. Maeter, F. Brückner, H.-H. Klauss, M. Nicklas, P. J. Baker, A. D. Hillier, M. Sigrist, A. Amato, and D. Johrendt, Phys. Rev. B **87**, 180503 (2013).
- ³⁰ M. H. Fischer, T. Neupert, C. Platt, A. P. Schnyder, W. Hanke, J. Goryo, R. Thomale, and M. Sigrist, Phys. Rev. B **89**, 020509 (2014).
- ³¹ X.-L. Qi, T. L. Hughes, and S.-C. Zhang, Phys. Rev. B **82**, 184516 (2010).
- ³² L. Mao, J. Shi, Q. Niu, and C. Zhang, Phys. Rev. Lett. **106**, 157003 (2011).
- ³³ M. Sato and S. Fujimoto, Phys. Rev. B **79**, 094504 (2009).
- ³⁴ A. Russo and S. Chakravarty, Phys. Rev. B **88**, 184513 (2013).
- ³⁵ T. Hyart, A. R. Wright, and B. Rosenow, Phys. Rev. B **90**, 064507 (2014).

- (2014).
- ³⁶ J. Röntynen and T. Ojanen, Phys. Rev. Lett. **114**, 236803 (2015).
 - ³⁷ J. Li, T. Neupert, Z. J. Wang, A. H. MacDonald, A. Yazdani, and B. A. Bernevig, arXiv:1501.00999.
 - ³⁸ L. Kimme and T. Hyart, Phys. Rev. B **93**, 035134 (2016).
 - ³⁹ C. Zhang, S. Tewari, R. M. Lutchyn, and S. Das Sarma, Phys. Rev. Lett. **101**, 160401 (2008).
 - ⁴⁰ M. Sato, Y. Takahashi, and S. Fujimoto, Phys. Rev. Lett. **103**, 020401 (2009).
 - ⁴¹ J. D. Sau, R. M. Lutchyn, S. Tewari, and S. Das Sarma, Phys. Rev. Lett. **104**, 040502 (2010).
 - ⁴² T. Jungwirth, J. Sinova, J. Mašek, J. Kučera, and A. H. MacDonald, Rev. Mod. Phys. **78**, 809 (2006).
 - ⁴³ T. Dietl and H. Ohno, Rev. Mod. Phys. **86**, 187 (2014).
 - ⁴⁴ A. Shitade and Y. Nagai, Phys. Rev. B **92**, 024502 (2015).
 - ⁴⁵ S. Murakami, N. Nagaosa, and S.-C. Zhang, Phys. Rev. B **69**, 235206 (2004).
 - ⁴⁶ J. M. Luttinger, Phys. Rev. **102**, 1030 (1956).
 - ⁴⁷ R. Winkler, *Spin-Orbit Coupling Effects in Two-Dimensional Electron and Hole Systems* (Springer, Heidelberg, 2003).
 - ⁴⁸ N. Read, Phys. Rev. B **79**, 045308 (2009).
 - ⁴⁹ N. Read and E. H. Rezayi, Phys. Rev. B **84**, 085316 (2011).
 - ⁵⁰ B. Bradlyn, M. Goldstein, and N. Read, Phys. Rev. B **86**, 245309 (2012).
 - ⁵¹ G. E. Volovik, *The Universe in a Helium Droplet* (Oxford University Press, New York, 2009).
 - ⁵² T. Ojanen, Phys. Rev. B **93**, 174505 (2016).